SAE TECHNICAL PAPER SERIES

921135

Visualization and Modeling of Factors Influencing Visibility in Computer-Aided Crewstation Design

Aries Arditi and Steven Azueta
The Lighthouse Inc.

James Larimer
NASA Ames Research Center

Michael Prevost
Sterling Software Inc.

Jeffrey Lubin and James Bergen
David Sarnoff Research Center

The Engineering Society For Advancing Mobility Land Sea Air and Space®
INTERNATIONAL

22nd International Conference on Environmental Systems
Seattle, Washington
July 13-16, 1992

400 COMMONWEALTH DRIVE, WARRENDALE, PA 15096-0001 U.S.A.

All SAE papers, standards, and selected books are abstracted and indexed in the SAE Global Mobility Database.

ISSN 0148-7191

Printed in USA

Visualization and Modeling of Factors Influencing Visibility in Computer-Aided Crewstation Design

Aries Arditi and Steven Azueta
The Lighthouse Inc.

James Larimer
NASA Ames Research Center

Michael Prevost
Sterling Software Inc.

Jeffrey Lubin and James Bergen
David Sarnoff Research Center

Abstract

We have developed two modules for use in computer-aided design (CAD) of crewstation environments that enhance the designer's appreciation of factors influencing the pilot's vision and visual processing capacity. The Binocular Optics Module (BOM) is an interactive tool for visualizing geometric aspects of 1) how retinal imagery of the environment changes on the pilot's retinas under conditions of eye and object motion, and 2) how visual capabilities that can be modeled as regions or contours on the retinas, affect spatial perception of the environment.

The Visual Performance Module (VPM) contains a signal processing model of human visual discrimination that quantitatively predicts visual discrimination performance. The outputs of the VPM are retinal contours that represent performance probabilities. These contours may be used as inputs to the BOM for visualizing those volumes of space within the crewstation that bound different levels of the pilot's of visual discrimination capability.

Used together, the BOM and VPM provide the designer with the opportunity to interactively explore relationships between environmental retinal imagery and visual function, and the ability to factor the pilot's visual capabilities into the earliest phases of crewstation CAD.

Introduction

Computer-aided design (CAD) of crewstations allows testing of many design concepts in a virtual environment. Allowing many design decisions to be made prior to building a physical prototype, CAD shortens development times and reduces costs.

While physical features and characteristics of materials are generally easy to build into a CAD system, human factors of the crewstation residents are more difficult, since these depend on anatomical, physiological, psychological and other systems about which we have less dependable information. Yet it would be highly desirable for the CAD tool to incorporate characteristics of the pilot, for example, into the design. The A^3I program at NASA-Ames, for example, has been pursuing the goal of building anthropometric models [5] into a crewstation CAD tool[1]. We have been exploring the feasibility of adding some of the pilot's visual capabilities to this A^3I effort[27].

Our software consists of two modules, an interactive Binocular Optics Module that that utilizes a simple model of binocular visual optics to explore the relationship between information on the retinas and environmental objects that form images on the retinas, and a Visual Performance Module (VPM) that predicts visual discrimination probabilities as a function of retinal location. Together the BOM and VPM provide the designer with a means of visualizing visual discrimination within the design space, rather than on the retinas. We now describe the BOM and VPM, and then illustrate how they can be used together by a crewstation designer.

Binocular Optics Module (BOM)

The BOM is the program through which the designer accesses the visual performance data, providing a visualization scheme described in greater depth elsewhere[4]. This visualization scheme itself incorporates a simple model of visual optics.

The BOM maintains two types of windows on the screen, one associated with the environment of this observer, the other associated with the observer's retinal imagery and retinal function. The former, which we call *WORLD* windows, describe the distal, while the latter *RETINA* windows describe the proximal, stimulus to vision. As the geometry of eye movements and of image formation in the eye are complex, the BOM uses a simplified model of visual optics. Figure 1 shows a half-tone rendition of one of the BOM's screens containing one *WORLD* and one *RETINA* window.

WORLD windows are perspective renditions of the observer's environment. Under default conditions, they contain only a rendition of a ground plane to aid the user in interpreting the perspective view, and a model of the observer's eyes with the lines of sight drawn to indicate

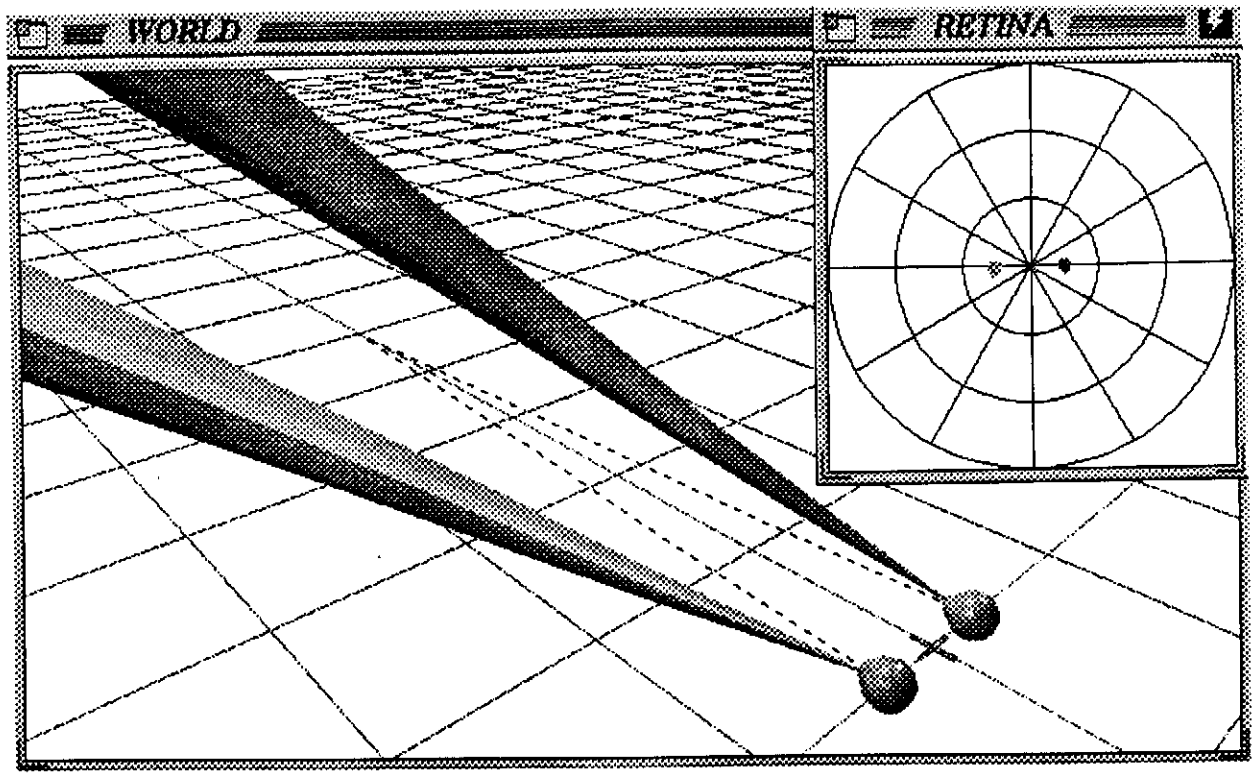

Figure 1: A screen of the BOM showing *WORLD* and *RETINA* windows. Shown here only in half-tones, color is used to code certain screen elements, with red and green coding retinal objects and retrojections imaged in or arising from the right and left eyes, respectively. Dashed lines indicate the visual axes; the long cones are retrojections of the normal blind spots.

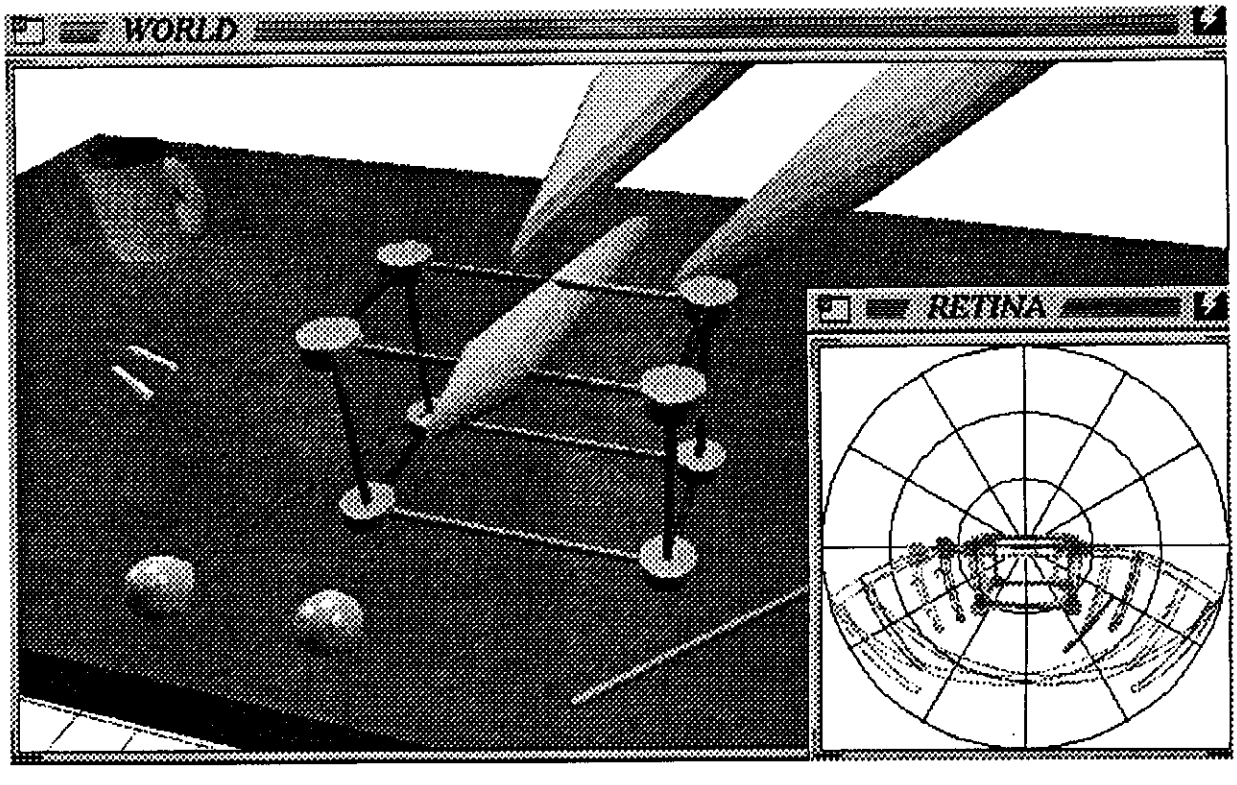

Figure 2: In this screen, the *WORLD* window depicts the eyes converged to the midpoint of the near top limb of the Tinker Toy. The three oblong structures are volume reconstructions of all possible intersections of retrojections at this viewing distance corresponding to the normal blind spots and a central disk of 10 deg diameter, that might represent, for example, an area of temporary blindness from foveal viewing of an intense flash of light. The *RETINA* window displays these retinal elements in addition to retinal imagery of *WORLD* objects.

	Direction in *RETINA* window			
	⟸		⟹	
Eye	Left	Right	Left	Right
Code	(Green)	(Red)	(Greeen)	(Red)
Visual Field	Temporal	Nasal	Nasal	Temporal
Retinal	Nasal	Temporal	Temporal	Nasal

Table 1: Horizontal coordinate conventions used in *RETINA* windows. The table shows, for each direction and eye represented in a window, the direction in conventional visual field or retinal coordinates. Also shown is color coding scheme for eye-of-origin of *RETINA* objects and retrojections.

the fixation position in the environment. A user typically adds graphic object models to the *WORLD* window to represent objects that are in the view, or potential view of the observer's eyes. A parser reads model descriptions from files conforming to the BOM's model description grammar. Model descriptions may be hierarchically defined, allowing the construction of arbitrarily complex models from more basic forms such as cubes, spheres, *etc.* In addition to the eyes, ground plane, and models representing objects in the visual environment, a *WORLD* window also has the capability to display what we term *retrojections* (see below).

When a *WORLD* window is active, the three-button mouse is used to change the location of the fixation point in space, and hence the positions of the eyes. Each button is associated with movement of the fixation point along one of the (x, y, or z) axes of the environment. In addition, the mouse can be used for changing the position of the center of projection and hence the viewpoint of the user in the *WORLD* environment.

RETINA WINDOWS – *RETINA* windows map graphic retinal objects either arising from retinal imagery or from two-dimensional retinal models of the user's creation, onto coordinate axes whose origin represents the observer's fovea. Generally, both retinas are represented superimposed ón a single window, with directions indicated as shown in Table 1.

Image objects are referred to as *projections*. Additionally, the BOM allows the construction of two-dimensional *RETINA* models, which generally indicate aspects of visual function. For example, a *RETINA* model might bound a central retinal region within which visual acuity exeeds some value. Or it might indicate a region of complete visual dysfunction (scotoma). In the current application (see below), *RETINA* objects are contours describing visual performance probabilities.

The major functions of *RETINA* windows are 1) to represent image motion on the retinas as the eyes move, and 2) to display shapes of *WORLD* object models as they would appear on the retina in the perimetric coordinates that are familiar to most users. As in human vision, if the eye moves to foveate an image point falling on eccentric retina on the map, the coordinates of that point must completely specify the direction and magnitude of the eye

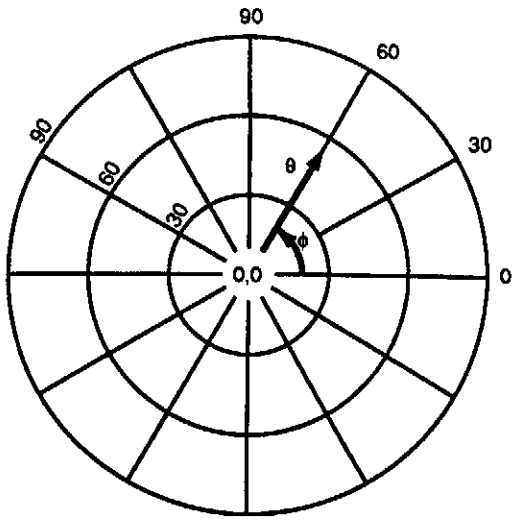

Figure 3: Listing coordinate system used in *RETINA* windows of the BOM.

movement required to fixate the point. In the BOM the Listing eye movement system of coordinates is adopted, where an eye movement from the primary position (eye straight ahead, head fixed and erect) is assumed to be accomplished by selection of a meridian ϕ (direction of rotation), rotation along that meridian to a parallel that corresponds to the magnitude of the eye movement θ, and rolling about the line of sight ω (see Figure 3). Good treatments of eye movement coordinate systems can be found in Alpern[3], Southall[26], or Hallett[17]. This system of axes is particularly convenient when Listing's law, which states that $\omega = 0$, is assumed, since, with the further assumption of a constant center of eye rotation, eye movements are completely determined with two degrees of freedom. Listing's law is generally found to hold approximately for normal observers, and especially for movements of less than about 25 deg (see Hallett [17], and is assumed in the BOM.

The particular projection chosen to represent the retina and associated eye in the default *RETINA* window is a zenithal equidistant projection of the Listing coordinate representation. Figure 3 is is an example of such a projection. Generally, the maps of both eyes are superimposed, to elucidate important features of the binocular field of view (see below). This projection is commonly used in visual perimetry and vision science, and is easy to comprehend, since the parallels are equidistant and denote visual angular distances from the fovea, or retinal eccentricity. Meridians of the map also faithfully indicate directions from the fovea. A further advantage of this projection is that its coordinates are linearly related to pixel and mouse position.

Several important aspects of vision are especially easy to appreciate in a *RETINA* window that displays the retinas of both eyes superimposed. First, where areas of permanent or transient retinal dysfunction are displayed, areas that are functional in at least one eye are displayed in red or green, or white. Where dysfunctional areas fall on corresponding locations in the two eyes, the intersection of those areas is displayed in yellow, indicating that this re-

gion of the binocular visual field is dysfunctional. Second, when retinal eccentricity of object imagery is different in the two eyes, one can visually compare eccentricity of the eye's images on the same coordinate map by comparing the red and green representations of the object. Third, since objects lying at distances removed from the fixation plane cast images on disparate retinal locations, the retinal disparity can be easily comprehended and computed directly from the map.

LINKING *WORLD* AND *RETINA* WINDOWS – Much of the power of the BOM lies in its ability to elucidate relationships between the proximal retinal visual stimulus, and the distal environmental stimulus. Figure 2 is an example of a screen that depicts such relationships, showing both retinal elements such as the blind spots and a central 10 deg dysfunctional region, in addition to retinal imagery of the world, viewed in wireframe. Figure 4 is another example, showing isodensity contours of human cone photoreceptors based approximately on the data of Curcio *et al.*[11].

Retinal image projection – In the BOM, *WORLD* object models can be rendered not only in *WORLD* windows, but in *RETINA* windows as well, to represent the optical image projections that take place in human vision. At present, projections are rendered only in wire-frame. Given a vertex $P = (x_p, y_p, z_p)$ of an object in space, and assuming that the optical node of the eye is at the origin, with the eye aligned with the positive z-axis, the coordinates (θ_p, ϕ_p) (see Figure 3) of P on the retina map in the *RETINA* window are:

$$\begin{aligned} \theta_p &= \sqrt{\lambda^2 + \mu^2} \\ \phi_p &= \arctan\left(\frac{\mu}{\lambda}\right), \end{aligned}$$

where $\lambda = arcsin\left(\frac{x_p}{\sqrt{x_p^2+z_p^2}}\right)$ and $\mu = arcsin\left(\frac{y_p}{\sqrt{y_p^2+z_p^2}}\right)$.

When the nodal point is not at the origin and the eye is rotated in an an arbitrary direction of fixation, retinal image vertices must be calculated with respect to the current location and orientation of the eye. *VP* maintains global coordinate transformations for each eye and computes retinal imagery with respect to these transformations.

Points between vertices undergo linear interpolation prior to projection so that shape on the retina map appropriately reflects shape on the retina, within the constraints of the zenithal equidistant projection.

Retrojections – While retinal images are projections of visual world objects onto the retinas, *VP* additionally performs a kind of converse operation that we call here *retrojection*. In retrojection, we begin with a retinal object point on the two dimensional retina map, and construct the locus of possible points in the visual world which may give rise, through projection, to that point on the retina. For a point on the retina, this point is always a line passing through the node of the eye. Given a point (ϕ_r, θ_r) on a retina map, define (λ_r, μ_r) as

$$\lambda_r = \theta_r \cos\phi_r$$

$$\mu_r = \theta_r \sin\phi.$$

The retrojection vector has arbitrary length $\rho = \sqrt{x_r^2 + y_r^2 + z_r^2}$, and a direction in space given by components

$$\begin{aligned} x_r &= \psi \tan\lambda \\ y_r &= \psi \tan\mu \\ z_r &= \psi, \end{aligned}$$

where $\psi = \sqrt{\frac{\rho^2}{\tan^2\lambda_r + \tan^2\mu_r + 1}}$. Analogously to projection, retrojections in other than the primary position are transformed by the global coordinate transformation of the eye.

Retrojections are displayed in the BOM in several ways. First, they may be displayed simply as lines of a constant radius selected by the user. Retrojected lines in this case fall on the inner surface of two hemispheres whose centers are the optic nodes of the eyes. Second, their intersections with any face of a *WORLD* object model polygon may be computed and displayed. This feature permits viewing retinal features directly on a surface being designed. For example, a designer wishing to view the locus of points within which either eye has sufficient visual acuity to read text on an indicator, may do so by using this feature. Third, the volume intersection of retrojections between the two eyes may be constructed and displayed. This permits the display, for example, of the volumes of space to which both eyes have reduced visibility as a result of disease, or temporary local retinal dysfunction.

THE VISUAL PERFORMANCE MODULE (VPM)

The VPM itself is a model of legibility that builds upon earlier one-dimensional discrimination models developed in basic and applied vision science [9, 10, 6, 32, 33, 31, 18, 15] and upon two-dimensional detection models developed by Watson and colleagues[28, 2, 24]

Figure 5 shows a block diagram of the basic model architecture. The model takes as input one or two retinal images produced by the BOM, and returns a prediction of the probability that an observer will be able to discriminate between the two images, or in the case of a single image input, that the observer will be able to discriminate between that image and a uniform field of the same mean luminance.

At the first stage, labeled "scaling" in the block diagram, the image is resampled according to the density of the cone mosaic. So for example, an image in the periphery of the visual field will be sampled more coarsely than an image at the fovea.

Next, in the contrast calculation stage, the raw luminance signal in the image is converted to units of local contrast as follows. First, the image is decomposed into a Laplacian pyramid[8], resulting in seven bandpass levels with peak frequencies from 32 through 0.5 cycles/degree,

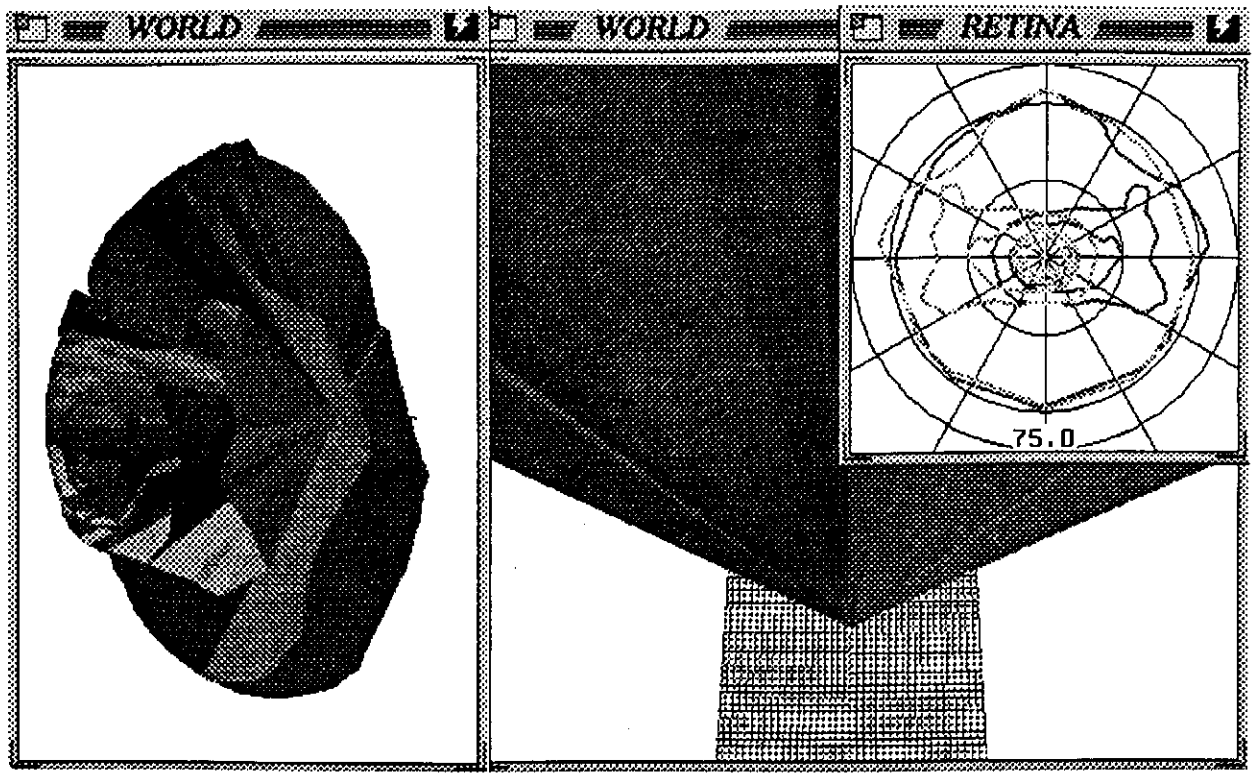

Figure 4: The *RETINA* window depicts contours of equal cone and hence photopic photoreceptor sampling density. *WORLD* windows show these contours retrojected into the environment, in a top view with ground plane (right) and side view (left). Other *WORLD* models are omitted for clarity.

each level separated from its neighbors by one octave. Then, at each point in each level, the pyramid value is divided by a local mean of image luminance. This local mean is the mean of a Gaussian filter applied at each point, of width corresponding to the pyramid at two levels broader than that on which the pyramid value is computed. The result is a measure of contrast, localized in both space and frequency. For a sine grating within the frequency range of one pyramid level, the resulting contrast measure is approximately equivalent to the Weber contrast; i.e., $(L_{\max} - L_{\min})/L_{\text{mean}}$. In the following stage, marked "oriented responses" in the diagram, each pyramid level is convolved with eight spatially oriented filters; i.e., a Hilbert transform pair for each of four different orientations. Then, the two Hilbert pair outputs at each point are squared and summed to compute a local energy measure for each orientation. For convenience and speed of operation, the linear filtering is performed with steerable filters of Freeman and Adelson[16]. The specific filters used are a second derivative of a Gaussian and its Hilbert transform, which have a log bandwidth at half height of approximately 0.7 octaves, a value within the range of bandwidths inferred psychophysically (e. g. [29]. The orientation bandwidth of these filters (i. e., the range of angles over which filter output is greater than one half the maximum) is approximately 65 degrees. This figure is slightly larger than the 40 degree tuning of monkey simple cells reported by Devalois et al.2b), and the 30 to 60 degree range reported psychophysically by Phillips and Wilson [25].

At the stage labeled "gain control," a gain-setting operation is performed on the four oriented energy responses e_j at each spatial point. This operation is

$$e'_j = \frac{e_j}{\alpha \sum_{k \neq j} e_k + 1}$$

where the subscripts j and k on the energy responses e index over the four different orientations for each spatial position and frequency. This formulation is supported by physiological data from Bonds[7] ; a similar expression was found by Lubin [20, 21] to fit psychophysical data using different spatio-temporally oriented patterns.

At the "transducer" stage, each energy measure e_i (where i indexes over position, frequency and orientation) is put through a sigmoid non-linearity of the form

$$T(e'_i) = \frac{r e_i'^{\frac{n}{2}}}{e'_i + s^2}$$

where n is a real number around 2.4, and s is a threshold parameter that indexes over frequency to set the contrast detection threshold at each frequency band. This nonlinearity T is required to reproduce the dipper shape of contrast discrimination functions [23].

Next, at the "pooling" stage, the spatial maps of transducer outputs are spatially averaged as an increasing function of eccentricity. This operation models an increasing spatial uncertainty in the localization of detected stimulus features, and is required to predict an eccentricity-dependent decrement in performance over that expected from loss in acuity alone, for tasks such as character discrimination [14] and bisection acuity [19]. This operation

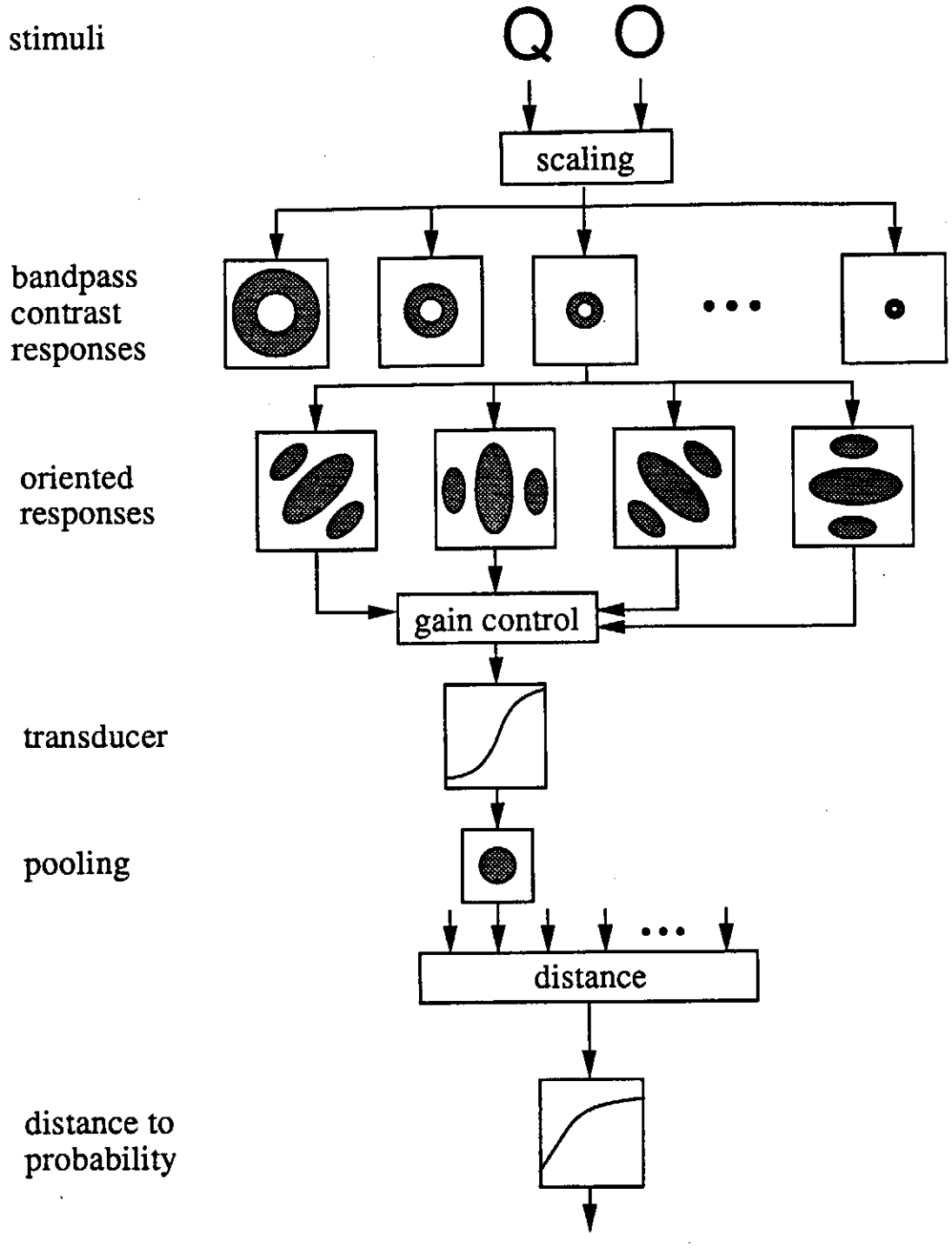

Figure 5: Flow diagram for VPM model (see text).

is supported by some physiological data [13, 22, for discussion].

Next, the set of m spatially averaged transducer outputs resulting from each of the two input images is treated as an m-dimensional vector, and a distance measure is calculated; i.e.,

$$D(s_1, s_2) = (\sum_{i=1}^{m} |T(e_i(s_1)) - T(e_i(s_2))|^Q)^{1/Q}$$

where s_1 and s_2 are the two images. For $Q = 2$, this expression returns the Euclidean distance between the two transducer output vectors. For $Q = \infty$,

$$D(s_1, s_2) = \max_{i=1}^{m} |T(e_i(s_1)) - T(e_i(s_2))|$$

a quantity which is not only faster to compute than an expression involving exponents, but is also more amenable to the fitting of various model parameters, since it effectively isolates each transducer channel from its neighbors. For the results to be reported here, Q was set to ∞. Although other similar models (e. g.[30] set Q to a value in the range of 2 to 4, the differences are minor for the results to be reported here; therefore we assumed $Q = \infty$ for computational convenience.

At the final stage, labeled "distance to probability," the computed distance measure is converted to a probability value, by applying the contrast associated with differences in transducer output to the contrast-to-probability mapping of a simple psychophysical contrast detection experiment (e.g. [15]). This value is returned by the model, and represents the probability that an observer would be able to detect a difference between the two input images.

This model can be calibrated to produce accurate performance predictions in grating contrast detection and discrimination tasks. When this is done, the model also produces accurate predictions on the edge sharpness discrimination data from Carlson and Cohen [9], without the need for further parameter adjustment. These predictions are shown in Figure 6.

Model performance in character discimination as a function of eccentricity is shown in Figure 7. Psychophysical data were obtained on the confusability of small (12 arc minutes width), briefly presented (167 msec), high contrast characters at different eccentricities. The subject was asked to choose "O" or "Q" on each trial, and the probability of correct identification was recorded. These data are shown as the filled symbols in Figure 7. The solid curve shows the predictions of the model. The observed fit is quite good.

Some differences exist between this and other discrimination models. For example in this model, a raw luminance signal is converted to contrast terms, whereas in many models the input signal is assumed to already be in contrast terms. Also, in the pyramid-based frequency decomposition used here, frequency and orientation bandwidths of the oriented mechanisms are constant across the different frequency bands, even though evidence suggests (e. g. [12] that bandwidths decrease as frequency increases. In other models (e. g.[30], the oriented linear filters

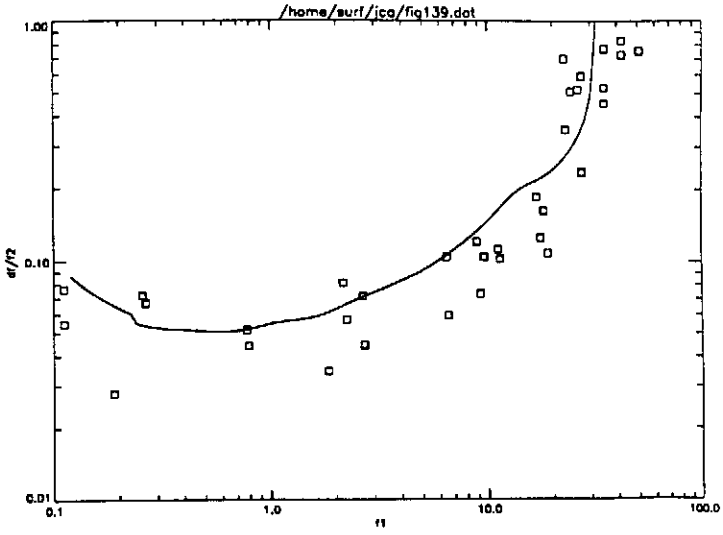

Figure 6: Data and model predictions for edge sharpness discrimination experiment. Data points show the minimum detectable change in the high frequency cut-off of a blurred step edge, as a function of the starting cut-off frequency. Solid curve shows the fit of the mechanistic model described in the text.

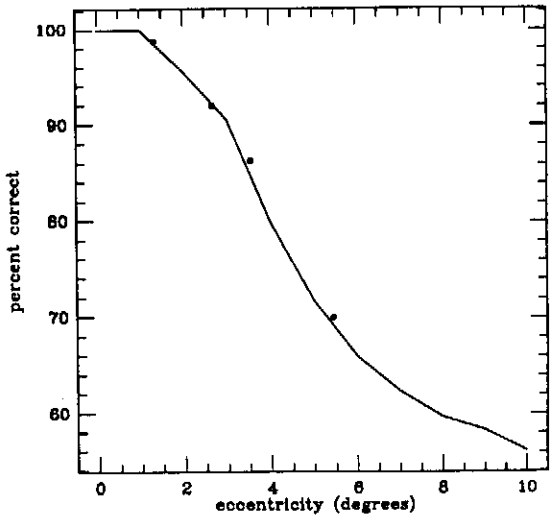

Figure 7: Data and model fits for discrimination of "O" and "Q" as a function of eccentricity. Solid symbols show the data. Dashed curve shows the predictions of a model with eccentricity-dependent pooling. Solid curve shows the predictions of a model with pooling and gain control among different orientations.

for different frequency bands vary in shape to take such data into account; the simplification was chosen here for efficiency of computation.

Using the BOM and VPM in Combination

Since visual discriminations are constrained for the most part by proximal visual factors such as the density of the retinal photoreceptor mosaic or variations in receptive field size across the visual field, it is natural that the outputs of the VPM should be in retinal coordinates. Practical manifestations of such constraints, however, are nearly always experienced by the user and are the concern of the designer in distal (environmental) space.

The BOM is used, in this context, to map retinotopic information about visual discriminations into the three-dimensional space of the crewstation, and to study the interplay of retinotopically mapped constraints with the geometrical constraints imposed by the location of the two eyes each with its own viewpoint and by the location of the components of the crewstation such as controls and indicators.

Figures 8 and 9 are examples of how a designer might visualize predictions of the VPM using the BOM. Both figures use the "Q" *vs.* "O"data shown in Figure 7. Figure 8 shows probability contours representing correct discrimination of these letters as a function of location in the visual field. These contours were generated by assuming that character discrimination was isotropic—that performance would depend only on retinal eccentricity, and not on retinal meridian. This allowed us to represent the discrimination probabilities as circular *RETINA* objects, with radii corresponding to their associated eccentric performance boundaries. For example, the contour of smallest radius represents the 0.99 performance probability: within this boundary, the model predicts that the observer will nearly always discriminate the "Q" from the "O." This view allows the designer to visualize, on the viewing surface being modeled (in this case the music stand), the predicted performance of the observer*.

Figure 9 illustrates the 0.75 performance probability taken from the same curve, but presented as a volume. This volume was reconstructed by the BOM from the intersections of the retrojections of the contour associated with this level of performance. In this type of view, one can visualize the volume of space which bounds a particular level of performance for both eyes, given the letter images are in good focus and are maintained at a constant angular size.

Conclusion

We have illustrated the main features of a visualization tool, the BOM, and of a predictive model of visual function, the VPM. Obviously this set of tools is only as accurate as the underlying models on which it relies. We are currently in the process of extending and refining both modules: The BOM will soon incorporate a simple model of eye movements and the capability to compute and display optic flow information. The VPM is being extended to predict a larger set of letter confusions, meridional variation, and discrimination of chromatic and temporally varying stimuli. Finally, better intercommunication of the two modules is planned in order to implement features such as binocular visibility enhancement effects. It is our hope that these modules will evolve into a simple and cost-effective CAD tool.

*Effects of binocular summation are not as yet taken into account in these predictions.

Acknowlegements

This work was supported by NASA-Ames cooperative agreement NCC2-541 and contract NAS2-12852.

References

[1] Army-NASA Aircrew/Aircraft Integration Program A^3I: Phase IV, man-machine integration design and analysis system (MIDAS) software detailed design document. TN-91-8216-0000, technical note 2, november. Technical report, Sterling Software, 1991.

[2] A. Ahumada, Jr. and A. Watson. Equivalent noise model for contrast detection and discrimination. *Journal of the Optical Society of America A*, 2:1133–39, 1985.

[3] M. Alpern. *The Eye*, chapter Movements of the Eyes. H. Davson (Ed.) Academic Press, New York, 1969.

[4] A. Arditi and S. Azueta. Visualization of 2-d and 3-d aspects of human binocular vision. Society for Information Display 1992 Symposium Digest of Technical Papers, in press.

[5] N. Badler. *Jack 4.8 User's Manual.* Computer Graphic Research Laboratory, University of Pennsylvania, 1990.

[6] P. G. J. Barten. The SQRI method: A new method for the evaluation of visible resolution on a display. In *Proceedings of the Society for Information Display*, pages 253–262, 1987.

[7] A. B. Bonds. Role of inhibition in the specification of orientation selectivity of cells in the cat striate cortex. *Visual Neuroscience*, 2:41–55, 1989.

[8] P. J. Burt and E. H. Adelson. The Laplacian pyramid as a compact image code. *IEEE Transactions on Communications*, COM-31:532–40, 1983.

[9] C. Carlson and R. Cohen. A simple psychophysical model for predicting the visibility of displayed information. In *Proceedings of the Society for Information Display*, pages 229–245, 1980.

[10] C. Carlson and R. Klopfenstein. Spatial frequency model for hyperacuity. *Journal of the Optical Society of America A*, 2:1747–51, 1985.

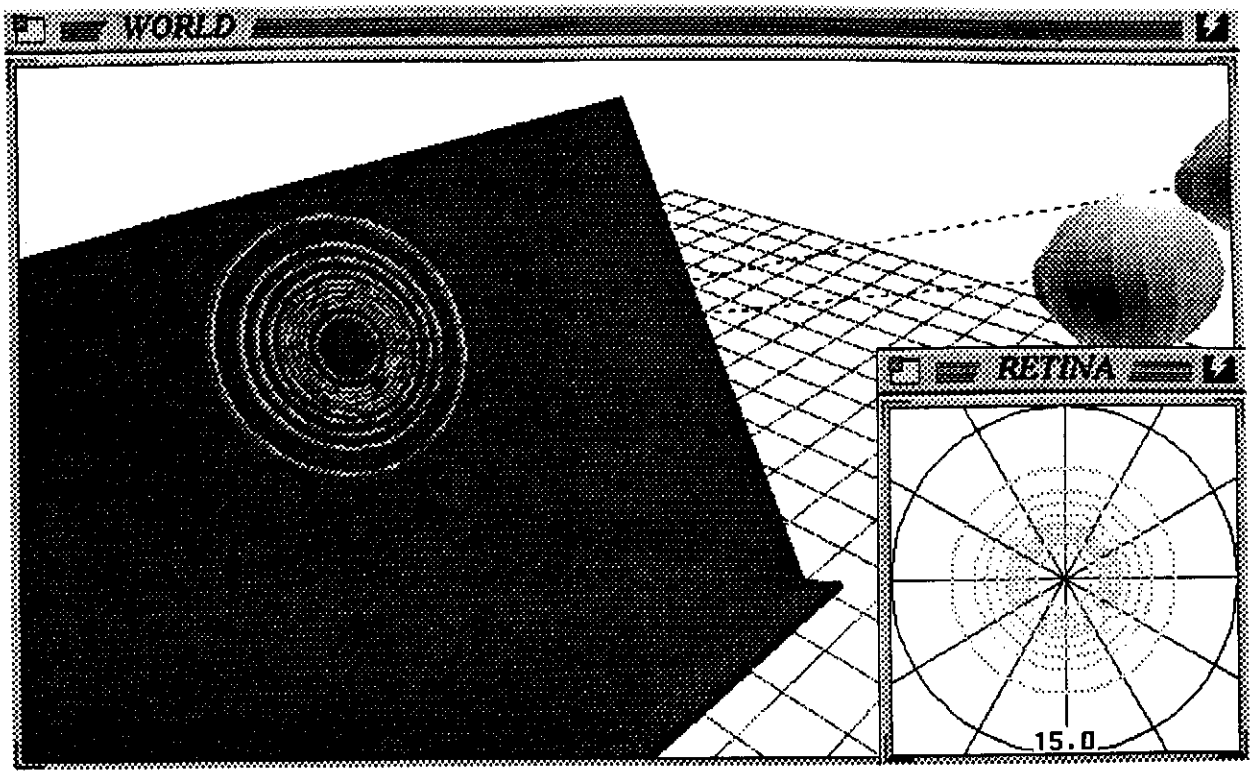

Figure 8: Retrojections of discrimination probabilities from the model that generated Figure 7 *projected* onto the hypothetical viewing surface of a music stand. With increasing eccentricity from the origin, the contours represent probabilities of 0.99, 0.95, 0.90, 0.85, 0.80, 0.75, 0.70, 0.65, 0.60, and 0.55 correct discrimination. Illumination on the display and display luminance were assumed by the model to be 10,000 ft C and 100 ft L, respectively.

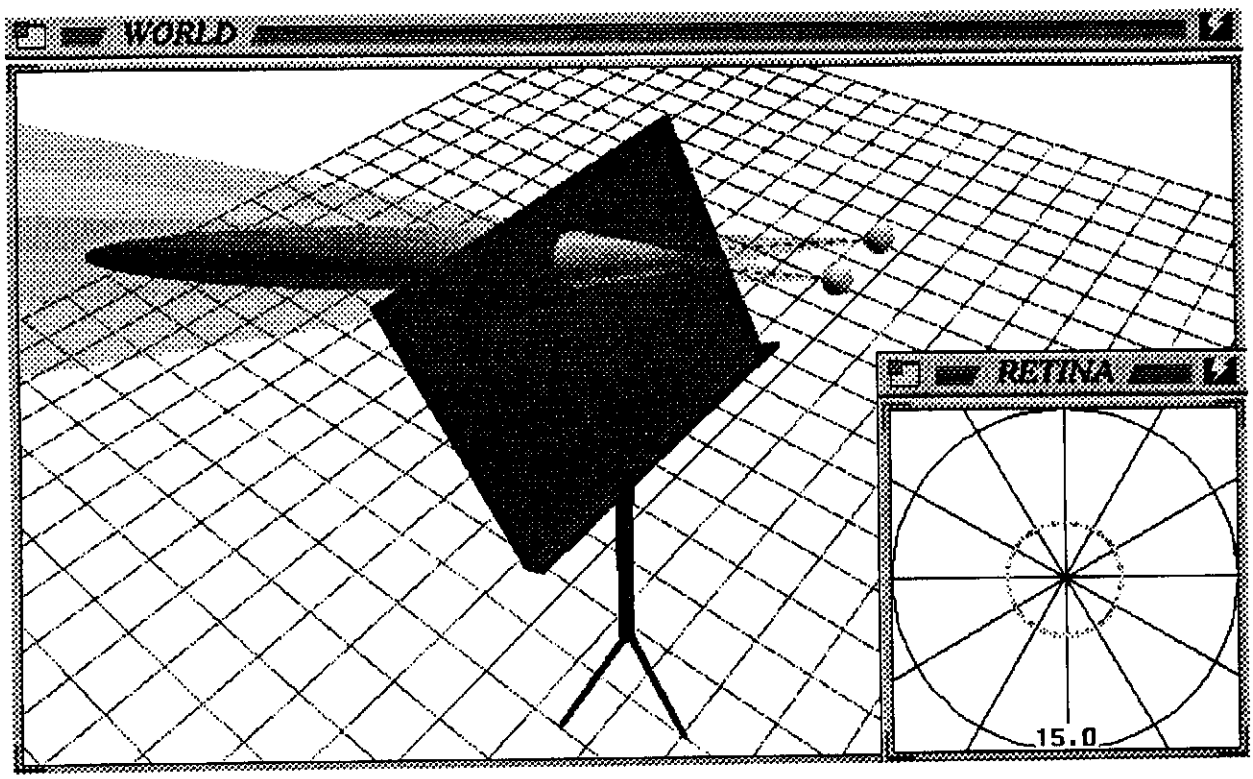

Figure 9: Volume reconstruction of intersection of left eye and right eye retrojections of 0.75 discrimination probability contour from Figure 8.

[11] C. A. Curcio, K. R. Jr. Sloan, O. Packer, A. E. Hendrickson, and R. E. Kalina. Distribution of cones in human and monkey retina: Individual variability and radial asymmetry. *Science*, 236:579–582, 1987.

[12] R. L. Devalois, D. G. Albrecht, and L. G. Thorell. Spatial frequency selectivity of cells in macaque visual cortex. *Vision Research*, 22:545–59, 1982.

[13] B. M. Dow, A. Z. Snyder, R. G. Vautin, and R. Bauer. Magnification factor and receptive field size in foveal striate cortex of the monkey. *Experimental Brain Research*, 44:213–28, 1981.

[14] J. E. Farrell and M. Desmarais. Equating character-identification performance across the visual field. *Journal of Optical Society of America A*, 7:152–59, 1990.

[15] J. M. Foley and G. E. Legge. Contrast detection and near-threshold discrimination in human vision. *Vision Research*, 21:1041–53, 1981.

[16] W. T. Freeman and E. H. Adelson. The design and use of steerable filters. *IEEE Transactions on Pattern Analysis and Machine Intelligence*, 13:891–906, 1991.

[17] P. E. Hallett. *Handbook of Perception and Human Performance*, chapter Eye Movements. K. Boff, L. Kaufman, and J. Thomas (Eds.) John Wiley and Sons, New York, 1986.

[18] G. E. Legge and J. M. Foley. Contrast masking in human vision. *Journal of the Optical Society of America*, 70:1458–71, 1980.

[19] D. M. Levi, S. A. Klein, and A. P. Aitsebaomo. Vernier acuity, crowding, and cortical magnification. *Vision Research*, 25:963–77, 1985.

[20] J. Lubin. Sub-additivity of masking among opponent motion signals. *Investigative Ophthalmology and Visual Science Supplement*, 29:251, 1988.

[21] J. Lubin. Discrimination contours in an opponent motion stimulus space. *Investigative Ophthalmology and Visual Science Supplement*, 30:426, 1989.

[22] J. Lubin and J. R. Bergen. Pattern discrimination in the fovea and periphery. *Investigative Ophthalmology and Visual Science Supplement*, 32:1024, 1991.

[23] J. Nachmias and R. V. Sansbury. Grating contrast: Discrimination may be better than detection. *Vision Research*, 14:1039–42, 1974.

[24] K. Nielsen, A. Watson, and A. Ahumada, Jr. Application of a computable model of human spatial vision to phase discrimination. *Journal of the Optical Society of America A*, 2:1600–06, 1985.

[25] G. C. Phillips and H. R. Wilson. Orientation bandwidths of spatial mechanisms measured by masking. *Journal of the Optical Society of America A*, 1:226–32, 1984.

[26] J. P. C. Southall. *Introduction to Physiological Optics*. Oxford University Press, London, 1937.

[27] Gary Stix. Human spec sheet. *Scientific American*, 265 (5):132–33, 1991.

[28] A. Watson. *Physical and Biological Processing of Images*, chapter Detection and recognition of simple spatial forms. O. Braddick and A. Sleigh (Eds.) Springer-Verlag, Berlin, 1983.

[29] A. Watson and J. G. Robson. Discrimination at threshold: Labelled detectors in human vision. *Vision Research*, 21:1115–22, 1981.

[30] H. R. Wilson. *Vision and Visual Dysfunction: Spatial Vision*, volume 10, chapter Psychopysical models of spatial vision and hyperacuity. D. Regan (Ed.) CRC Press, Inc., Boston, 1991.

[31] H. R. Wilson and J. R. Bergen. A four mechanism model for threshold spatial vision. *Vision Research*, 19:19–32, 1979.

[32] H. R. Wilson, D. K. McFarlane, and G. C. Phillips. Spatial tuning of orientation selective units estimated by oblique masking. *Vision Resarch*, 23:873–882, 1983.

[33] H. R. Wilson and D. Regan. Spatial frequency adaptation and grating discrimination: predictions of a line element model. *Journal of the Optical Society of America A*, 1:1091–96, 1984.